Flexural Response of GFRP-Reinforced Geopolymer Concrete Beams

Ginghis B. Maranan[1], Allan C. Manalo[2], Warna Karunasena[3], Brahim Benmokrane[4], and Priyan Mendis[5]
[1]PhD Candiate, University of Southern Queensland
[2]Senior Lecturer, University of Southern Queensland
[3]Professor, University of Southern Queensland
[4]Professor, University de Sherbrooke
[5]Professor, The University of Melbourne

Abstract: This study investigated the flexural response of glass fibre reinforced polymer-reinforced geopolymer concrete (GFRP-RGC) beams using a four-point static bending test. Three full-scale beams were cast and reinforced with nearly same amount of longitudinal GFRP reinforcements but of varying diameters at the bottom (4-12.7 mm, 3-15.9 mm, and 2-19.0 mm), two 12.7 mm GFRP bars at the top, and 9.5 mm GFRP stirrups spaced at 100 mm on-centre. The average compressive strength of the geopolymer concrete was 38.2 MPa. Based on the experimental results, all the tested beams showed nearly similar crack pattern, load-deflection response, bending-moment and deflection capacities, and strain readings, suggesting that the flexural response of a GFRP-RGC beam was not significantly influenced by the bar diameter; instead, by the properties of the geopolymer concrete. The $0.3M_u$ criterion suggested by Bischoff must be adapted in the serviceability design of a GFRP-RGC beam. The flexural capacities of the tested beams were generally higher than the predicted values from ACI 440.1R-06 and CSA S806-12 standards. Furthermore, the GFRP-RGC beams have higher strength compared with their GFRP-reinforced concrete counterparts. Thus, it can be concluded that the GFRP-RGC beams have structural properties that are suitable for civil infrastructure applications.

Keywords: flexural response, geopolymer concrete, GFRP bars, four-point static bending test, civil infrastructure.

1. Introduction

Cement-based concrete is one of the oldest and most commonly used construction materials in the world. The demand for this material is expected to increase in the future owing to rise of infrastructure need by many developing countries and the growing number of old and deteriorated concrete structures needing urgent repair and rehabilitation. The production of cement, however, contributes billions of tons of waste materials and about 7% of the world's greenhouse gas yearly (1). In fact, several studies revealed that for every 1.0 tonne of cement produced, approximately 1.0 tonne of CO_2 are being released into the atmosphere (2). With the alarming increase of Earth's average surface temperature due to greenhouse gases, also known as global warming, the construction industry, specifically, are prompted to replace cement with a greener material like geopolymer. Geopolymer is a highly sustainable concrete binder as it can be manufactured using by-product materials, like fly ash and blast furnace slags. Davidovits (3) proposed the term "geopolymer" since the chemical reaction that takes place between the aluminum (Al) and silicon (Si) source material and the alkaline liquid activator is a polymerization process.

Many studies have shown that geopolymer concrete has physical and mechanical properties that are suitable for structural applications (4-6). In fact, the geopolymer concrete internally reinforced with steel bars has been successfully utilised in the construction of several civil infrastructures such as pavement, retaining walls, and bridges. However, in order to maximize its full potential for various structural applications especially in harsh environment, the corrosion of steel reinforcements must be avoided or must be eliminated, if possible, since this phenomenon results in geopolymer concrete cracking and spalling that can lead to early strength degradation and loss of serviceability of the structure before reaching its expected service life. Among the possible solutions that are being implemented to address this concern is to utilise fibre reinforced polymer (FRP) bars because, aside from being corrosion-resistant, these bars have high tensile strength, lightweight, high fatigue endurance, electromagnetic neutrality, and have low thermal and electrical conductivity (7).

With the advantageous properties of the geopolymer concrete and the FRP bars, their combination can be anticipated to yield a construction technology that is both more sustainable and more durable with adequate structural integrity. Limited studies, however, are available that deals with FRP-reinforced

geopolymer concrete and this has been the key motivation of this undertaking. This study presents an investigation of the flexural response of geopolymer concrete beams reinforced with sand-coated glass FRP (GFRP) bars subjected to four-point static bending test. Three full-scale beams with nearly same amount of bottom GFRP bars but with varying diameter were cast and tested. The crack patterns and failure modes, load versus deflection relationships, bending-moment and deflection capacities, and strains in the bars and geopolymer concrete are presented. Furthermore, the experimental flexural capacity of beams are compared with the predicted values using the current standards and with their GFRP-reinforced concrete (GFRP-RC) counterparts to verify the suitability of the proposed system for structural applications.

2. Experimental Program

2.1 Materials and test specimens

Three high modulus (HM) sand-coated GFRP bars with nominal diameters (d_b) of 12.7 mm, 15.9 mm, and 19.0 mm were used to longitudinally reinforce the beams (Figure 1). The bars, as shown in Figure 1, were produced through the pultrusion process of E-Glass fibres impregnated in a thermosetting modified vinyl ester resin (Grade III, CSA S807-10 (8)). Table 1 summarises the physical and mechanical properties of the bars as provided by the manufacturer, including the guaranteed tensile strength (f_{fu}) and elastic modulus (E_f), computed based on the nominal area (A_f), and the usable strain (ε_{cu}).

The geopolymer concrete used in the study was made up of fly ash and slag, fine and medium sands, 10 mm and 20 mm coarse aggregates, water, and alkaline liquid. Table 2 presents the mechanical properties of the geopolymer concrete. Based on the compression test of four 100 mm diameter by 200 mm high cylinders, the average 28-day compressive strength (f'_c) and elastic modulus (E_c) of the geopolymer concrete were 38 MPa and 38.5 GPa, respectively. Furthermore, the three-point static bending test of the three geopolymer concrete prisms (75 mm x 75 mm x 285 mm) yielded an average modulus of rupture (f_r) of 3.86 MPa.

Three full-scale geopolymer concrete beams were cast and tested. The beams were longitudinally reinforced at the bottom with 4-12.7 mm, 3-15.9 mm, and 2-19.0 mm HM GFRP bars. Furthermore, each beam was provided with 2-12.7 top HM GFRP bars and 9.5 mm HM GFRP stirrups spaced at 100 mm on-center. The beams were 200 mm wide, 300 mm deep, and 3100 mm long and were designed as over-reinforced to achieve a concrete crushing failure mode. Figure 2 shows the beams' cross-sectional geometry and reinforcement details while Table 3 summarises the label and classification of each beam in accordance with their bottom longitudinal reinforcements. The actual and balanced reinforcement ratio (ρ_f and ρ_{fb}, respectively) were calculated using Equations 1 and 2. The terms α_1 and β_1 were obtained from Equation 3 for ACI 440.1R-06 (9) and from Equation 4 for CSA S806-12 (10). These equations are summarised in Table 8. The maximum usable strain of the geopolymer concrete (ε'_{cu}) were assumed to be 0.003 and 0.0035 for ACI 4401.R-06 and CSA S806-12, respectively.

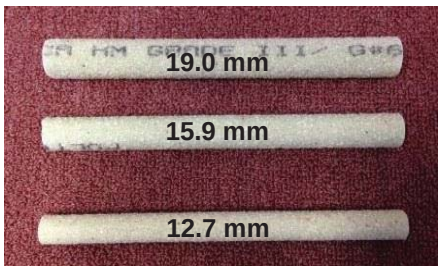

Figure 1. GFRP Bars.

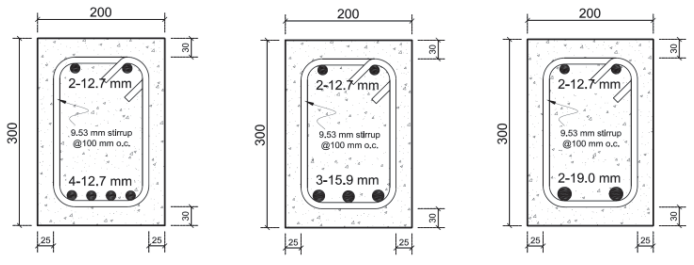

(a) GFRP-RGC-4-12.7 (b) GFRP-RGC-4-12.7 (c) GFRP-RGC-4-12.7

Figure 2. Cross-sectional geometry and reinforcement details of the beams.

Table 1. Properties of GFRP bars.

d_b (mm)	A_f (mm^2)	f_{fu}^* (MPa)	E_f (GPa)	ε_{cu} (με)
9.5	71	1029	50	20580
12.7	129	1312	65.6 ± 2.5	20000
15.6	199	1184	65.6 ± 2.5	18914
19.0	284	1105	65.6 ± 2.5	17347

**Guaranteed tensile strength: Average value – 3X standard deviation (ACI 440.1R-06)*

Table 2. Properties of geopolymer concrete.

f'_c (MPa)	E_c (GPa)	f_r (MPa)
38.2	38.5	3.86

Table 3. Label and classification of the tested beams.

Beam	Section		Tension Reinforcement				Remarks
	b (mm)	h (mm)	#	d_b (mm)	ρ_f (%)	$\rho_{fb}^\dagger$ (%)	
GFRP-RGC-4-12.7	200	300	4	12.7	1.13	0.38 (0.40)	Over-reinforced
GFRP-RGC-3-15.9	200	300	3	15.9	1.18	0.33 (0.35)	Over-reinforced
GFRP-RGC-2-19.0	200	300	2	19.0	1.00	0.29 (0.30)	Over-reinforced

2.2 Test method and instrumentations

Figure 3 shows the schematic diagram of the four-point static bending test employed in the study. The beams were loaded at midspan with two concentrated loads spaced at 400 mm, yielding a shear span of 1100 mm on both sides. The load was applied using a 2000 kN capacity hydraulic jack at a rate of approximately 3 mm/min. The midspan deflection was measured using a Laser Optical Displacement (LOD) device. Furthermore, electrical strain gauges were attached to the top surface of the geopolymer concrete beam and in the top and bottom reinforcements to measure the longitudinal strains during loading. The loads and strain readings were captured using the System 5000 data logger.

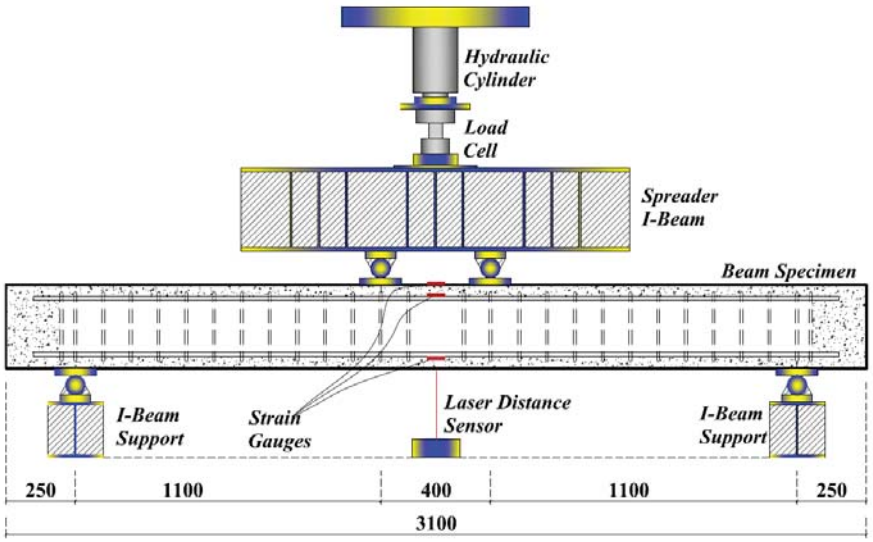

Figure 3. The four-point static bending test.

3. Results and Discussion

3.1 Experimental results

3.1.1 Crack pattern and failure mode

All the tested beams were initially uncracked before loading. Then, several vertical cracks were formed along their constant bending-moment zone right after the applied load exceeded the geopolymer concrete tensile capacity. With further loading, these cracks became wider and propagated upward while new flexural cracks were developed on both shear spans of the beams. At higher loads, the vertical cracks within the pure bending zone further widen while the vertical cracks on both shear spans became more inclined due to the shear stresses. However, the rate of lengthening and widening of inclined cracks did not increase as the geopolymer concrete began to crush. At the final loading stage, few inclined cracks reached the crushed zone of the geopolymer concrete. Figure 4 shows the final crack patterns of the tested beams. Based on the figure, the cracks were almost uniformly distributed along the beam span with spacing of approximately 100 mm, similar to stirrups spacing. This observation demonstrated that a composite action existed between the GFRP bars and the geopolymer concrete, that is the stress is effectively transfer from geopolymer concrete to GFRP bars and vice versa, through the friction and mechanical interlock provided by sand-coats. No significant difference can be observed among the crack patterns of the beams.

Figure 5 depicts the typical failure mode of the tested beams. As expected, the over-reinforced beams failed in flexure through crushing of the geopolymer concrete in the compression zone. Gangarao et al. (7) reported that, generally, the preferred failure mode for any FRP reinforced concrete beam is the concrete crushing since this failure is more gradual, less brittle, and less catastrophic with higher deformability compared with the FRP tensile rupture. Thus, it can be concluded that the tested beams were designed satisfactorily and accordingly.

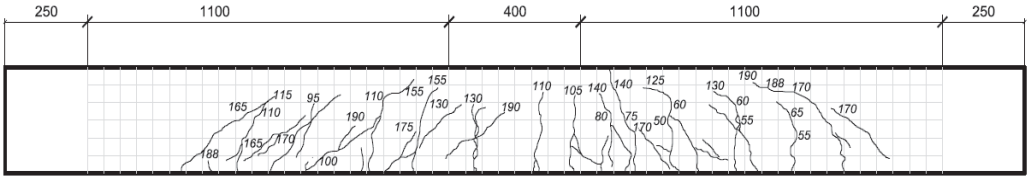

(a) GFRP-RGC-4-12.7

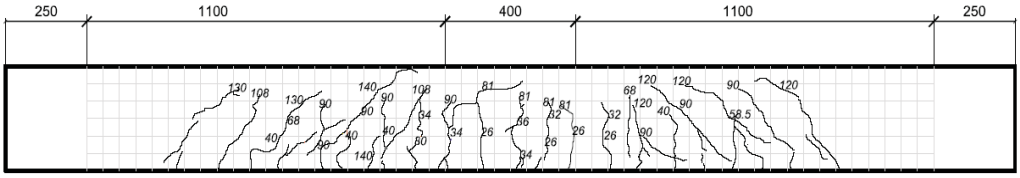

(a) GFRP-RGC-3-15.9

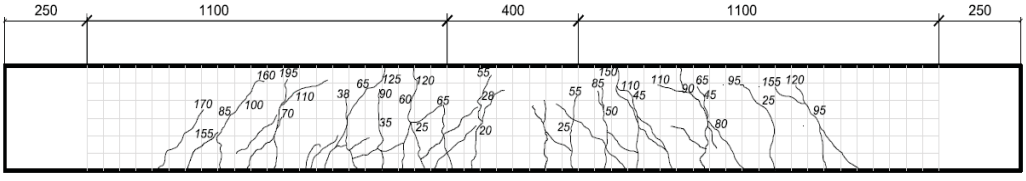

(a) GFRP-RGC-2-19.0

Figure 4. Crack patterns of the tested beams.

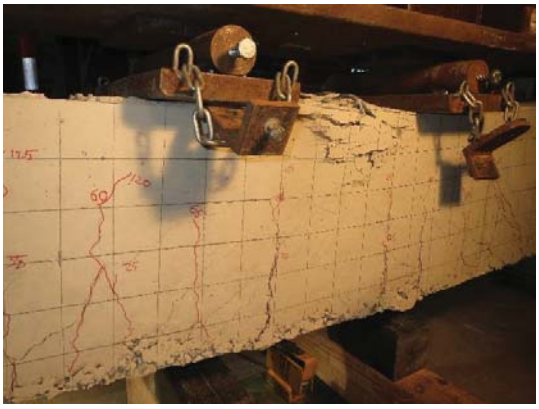

Figure 5. Typical failure mode of the tested beams.

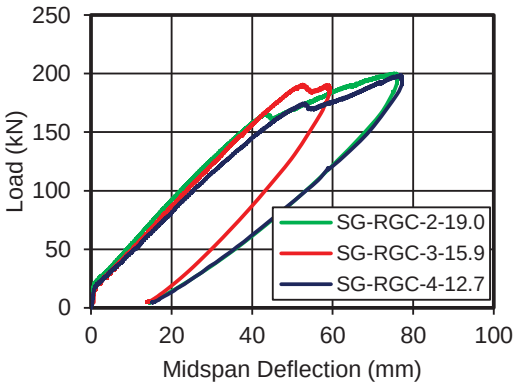

Figure 6. Load-deflection response of the tested beams.

3.1.2 Load-deflection response

Figure 6 shows the relationship between the applied load and the midspan deflection of the tested beams. Generally, their load-deflection curves can be divided into three segments. The first segment embodies the typical steep linear response of an uncracked beam, wherein the load increases linearly with midspan deflection. This section is similar for all beams no matter the amount and type of reinforcements, because at this stage, only the geopolymer concrete is sustaining all the applied loads. The second segment represents the cracked response of the beam. It is composed of a linear response with reduced slope, similar for all the tested beams, followed by a non-linear response up until the crushing failure of the geopolymer concrete in the compression zone. This non-linearity can be attributed to extensive cracking and crushing of the geopolymer concrete. Lastly, the third segment represents the post-failure response of the beam wherein the beam continued to sustain additional loads after the crushing failure of the geopolymer concrete, owed to the stirrup confinement effect that enhanced the ductility and strength of the beams. The slope of this segment is lower than the previous segment due to the initiation of failure in the GFRP bars.

The beams were loaded just before its final failure to avoid any mishaps during testing. The behaviour during load removal was also recorded. The unloading segment showed the inherent elastic characteristic of the beams at higher loads, even after exhibiting a nonlinear behaviour or even after the concrete crushing failure.

3.1.3 Bending-moment capacity

Table 4 summarises the experimental flexural capacity of the tested beams at geopolymer concrete cracking ($M_{cr\text{-}exp}$), at service condition ($M_{s\text{-}exp}$), at geopolymer concrete crushing failure ($M_{u\text{-}exp}$), and at peak ($M_{peak\text{-}exp}$). The $M_{cr\text{-}exp}$ was determined based on the recorded load when the first flexural crack appeared and was verified from load-deflection and moment-strain plots of beams. The GFRP-RGC-4-12.7, GFRP-RGC-3-15.9, and GFRP-RGC-2-19.0 beams yielded nearly similar $M_{cr\text{-}exp}$ values of 10.4 kN-m, 11.5 kN-m, and 11.9 kN-m, respectively. This can be expected since the $M_{cr\text{-}exp}$ is mainly dependent on the geopolymer concrete properties. The marginal difference can be attributed to the nonhomogeneous and anisotropic properties of the geopolymer concrete. The average cracking moment and the corresponding modulus of rupture (f_r) were 11.3 kN-m and 3.76 MPa, respectively. This value of f_r was comparable to that obtained from the bending test of geopolymer concrete prisms.

In this study, the suggested criteria by ISIS-06 (11) and Bischoff et al. (12) were used to identify the $M_{s\text{-}exp}$ of the beams. The first benchmark defines the $M_{s\text{-}exp}$ as the bending-moment value that

corresponds to a tensile-strain reading of 2000 με in the reinforcement, the specific strain value that limits the crack width to 0.7 mm and 0.5 mm for interior and exterior exposures, respectively, in any FRP-RC components. The second benchmark, on the other hand, approximates $M_{s\text{-}exp}$ as 30% of a beam's ultimate capacity ($0.3M_{u\text{-}exp}$). Based on these criteria, all the tested beams yielded comparable $M_{s\text{-}exp}$ values except that of GFRP-RGC-3-15.9 beams at 2000 με.

The $M_{u\text{-}exp}$ of GFRP-RGC-4-12.7, GFRP-RGC-3-15.9, and GFRP-RGC-2-19.0 were 96.1 kN-m, 104.8 kN-m, and 91.4 kN-m, respectively. These values were relatively comparable to each other, suggesting that the nominal diameter does not influence the beams' bending-moment capacity, mainly because the failure of these beams was governed by geopolymer concrete crushing failure and not by tensile rupture of the GFRP bars. The slight variation can be attributed to, again, the intrinsic composite characteristic of the geopolymer concrete. All the tested beams, however, continued to sustain further loads even after the crushing failure and yielded another peak bending-moment, owed to the confinement effect provided by GFRP stirrups located in the constant bending-moment zone. The $M_{peak\text{-}exp}$ were 109.3 kN-m, 104.7 kN-m, and 110.1 kN-m for GFRP-RGC-4-12.7, GFRP-RGC-3-15.9, and GFRP-RGC-2-19.0, respectively. The 25 mm gap, between the beam and the load applicator, prior to load application resulted in a relatively lower $M_{peak\text{-}exp}$ of GFRP-RGC-3-15.9 compared with the other beams. Thus, it can be further concluded that the nominal bar diameter have no significant effect on beam strength even after crushing failure.

Table 4. Flexural capacity and failure mode of the tested beams.

Beam	$M_{cr\text{-}exp}$ (kN-m)	$M_{s\text{-}exp}$ (kN-m)		$M_{u\text{-}exp}$ (kN-m)	$M_{u\text{-}theo}$ (kN-m)†		$M_{peak\text{-}exp}$ (kN-m)	Failure Mode
		2000 με	$0.30M_{u\text{-}exp}$		ACI 440.1R-06	CSA S806-12		
GFRP-RGC-4-12.7	10.4	27.2	28.8	96.1	71.5 [74%]	77.2 [80%]	109.3	Concrete crushing
GFRP-RGC-3-15.9	11.5	21.3	31.4	104.8	73.9 [71%]	79.7 [76%]	104.7	concrete crushing
GFRP-RGC-2-19.0	11.9	27.0	27.4	91.4	72.3 [79%]	78.0 [85%]	110.1	concrete crushing

†*The number inside [ ] represents the ratio between* $M_{u\text{-}theo}$ and $M_{u\text{-}exp}$

3.1.4 Midspan deflection

Table 5 shows the midspan deflection at service load level ($\Delta_{s\text{-}exp}$), at geopolymer concrete crushing failure ($\Delta_{u\text{-}exp}$), and at unloaded phase or residual deflection ($\Delta_{res\text{-}exp}$) of tested beams. As discussed earlier, the serviceability performance of the beams was described based on ISIS-07 and Bischoff et al.'s suggestions. The recorded $\Delta_{s\text{-}exp}$ based on ISIS (Bischoff) criterion were 10.6 mm (11.5 mm), 7.1 mm (12.3 mm), and 8.7 mm (8.8 mm) for GFRP-RGC-4-12.7, GFRP-RGC-3-15.9, and GFRP-RGC-2-19.0, respectively. It was evident from these results that the nominal bar diameter have no significant correlation on the serviceability performance of the beams since the measured $\Delta_{s\text{-}exp}$ for each criterion was comparable to each other. Generally, all the tested beams satisfy the deflection limit set by the ACI 440.1R-06, which is equivalent to L/240 or 10.8 mm. However, the results showed that the serviceability design of a GFRP-RGC beam should be based on $0.3M_{u\text{-}exp}$ criterion since the estimated deflections based on this criterion were higher than that of ISIS. El-Nemr et al. (13) also adapted the same criterion for the serviceability design of FRP-RC beams.

The $\Delta_{u\text{-}exp}$ of GFRP-RGC-4-12.7, GFRP-RGC-3-15.9, and GFRP-RGC-2-19.0 were 53.2 mm, 52.5 mm, and 43.4 mm, respectively. From these results, it can be concluded that the deflection behaviour of GFRP-RGC beam is not dependent on the bar diameter. All the tested beams yielded similar $\Delta_{res\text{-}exp}$ values, having an average of 14.3 mm. This magnitude of residual deflection shows the inherent elastic behaviour of the GFRP-RGC beams at higher loads, even after the crushing failure of the geopolymer concrete.

Table 5. Midspan deflection of the tested beams.

Beam	$\Delta_{s\text{-}exp}$ (mm)		$\Delta_{s\text{-}theo}$ (mm)†		$\Delta_{u\text{-}exp}$ (mm)	$\Delta_{u\text{-}exp}$ (mm)†		$\Delta_{res\text{-}exp}$ (mm)
	2000 με	$0.30M_{u\text{-}exp}$	2000 με	$0.30M_{u\text{-}exp}$		ACI 440.1R-06	CSA S806-12	
GFRP-RGC-4-12.7	10.6	11.5	7.4	8.2	53.2	36.3	35.3	15
GFRP-RGC-3-15.9	7.1	12.3	3.6	8.3	52.5	36.3	35.7	14
GFRP-RGC-2-19.0	8.7	8.8	6.6	6.8	43.4	32.9	32.9	14

†*Based on ACI 440.1R-06*

3.1.5 Strain in the longitudinal reinforcement and geopolymer concrete

Figure 7 shows the moment-strain relationships of the tested beams. Analogous moment-strain curvatures occurred among top bars (TB), bottom bars (BB), and geopolymer concrete (GC). Furthermore, the top and bottom reinforcements yielded trilinear curves, similar to the load-deflection curve, while the geopolymer concrete only yielded a bilinear curve because the strain gauge attached on geopolymer concrete's top surface did not provide further readings after its crushing failure. These observations tend to show that no slippage occurred during the test, thereby demonstrating the effectiveness of anchoring the GFRP bars in geopolymer concrete using sand-coatings.

Table 6 shows the strain readings at service condition based on $0.3M_{u\text{-}exp}$, at geopolymer concrete crushing failure, and at peak. The strains at bottom bars were all greater than 2000 με, showing the appropriateness of using Bischoff's criterion for the GFRP-RGC beam serviceability design. On other hand, the maximum usable strain in the geopolymer concrete reached a magnitude of 4831 με that is higher than those normally assumed in ACI 440.1R06 and CSA S806-12 standards. The peak tensile strain at the bottom bars were just 79 %, 79 %, and 86 % of the bars' tensile capacity for GFRP-RGC-4-12.7, GFRP-RGC-3-15.9, and GFRP-RGC-2-19.0, respectively. All the tested beams yielded nearly comparable strains at different load stages that further verified that bar diameter have no significant effect on the flexural performance of the GFRP-RGC beam.

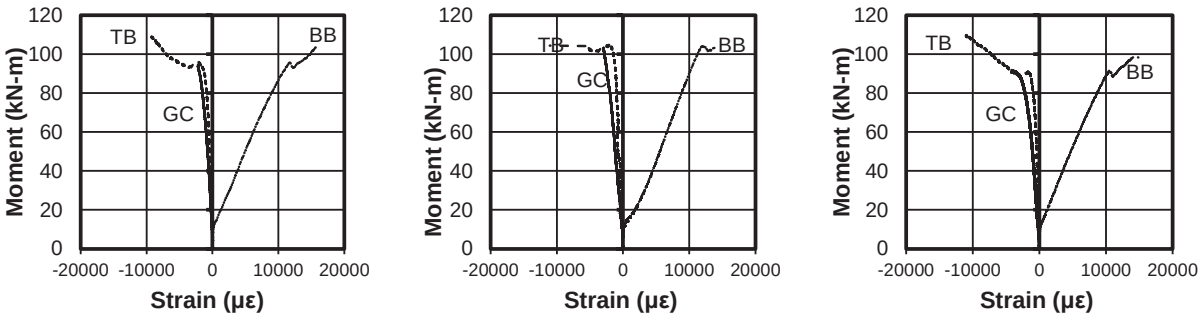

(a) GFRP-RGC-4-12.7 (b) GFRP-RGC-3-15.9 (b) GFRP-RGC-3-15.9

Figure 7. Moment-strain relationships of the tested beams.

Table 6. Strains in geopolymer concrete (GC), top bars (TB), and bottom bars (BB).

Beam	At service condition (με)			At failure (με)			At peak (με)	
	GC	TB	BB	GC	TB	BB	TB	BB
GFRP-RGC-4-12.7	348	247	2147	4831	2327	11547	9271	15746
GFRP-RGC-3-15.9	698	156	3508	2934	2115	12244	11083	14956
GFRP-RGC-2-19.0	502	203	2028	4226	2086	10855	11186	14963

†*Based on ACI 440.1R-06*

3.2 Theoretical Prediction

Table 7 shows the summary of the equations, suggested by ACI 440.1R-06 and CSA S806-12 standards, used in the study. The theoretical flexural capacities of the beams at geopolymer concrete crushing failure ($M_{u\text{-}theo}$) were computed using Equation 5 and were summarized in Table 4. The stress in the bar (f_f) was calculated from Equation 6 for ACI 440.1R-06 and from Equation 7 for CSA S806-12, where the neutral axis c was determined from Equation 8. The $M_{u\text{-}theo}$ based on ACI 440.1R-06 were 71.5 kN-m, 73.9 kN-m, and 72.3 kN-m for GFRP-RGC-4-12.7, GFRP-RGC-3-15.9, and GFRP-RGC-2-19.0, respectively, while CSA S806-12 yielded 77.2 kN-m, 79.7 kN-m, and 78.0 kN-m, respectively. Generally, the prediction equations underestimated the flexural capacity of the tested beams due to several factors. First, the ε'_c used in the prediction, such as 3000 με for ACI 440.1R-06 and 3500 με for CSA S806-12, were lower compared with the actual strain that can reach a value of 4831 με. Second, the flexural contribution of top GFRP bars was neglected in both equations. Finally, the confinement effect due to later ties provided in the pure bending-moment zone were not considered. By comparing the two standards, the CSA S806-12 yielded more accurate results than the ACI 440.1R-06.

The predicted midspan deflection at service condition ($\Delta_{s\text{-}theo}$) and at geopolymer concrete crushing failure ($\Delta_{u\text{-}theo}$) were shown in Table 5. These values were calculated from Equations 9, 10, and 11 for ACI 440.1R-06 and from Equations 12 and 13 for CSA S806-12. The computed $\Delta_{s\text{-}theo}$ and $\Delta_{u\text{-}theo}$ were lower than their actual deflection counterparts. The underestimation, however, was more evident at higher applied loads, owing to the overestimation of the tension stiffening parameter.

Table 7. Summary of equations used for theoretical predictions.

ACI 440.1R-06	CSA S806-12
$\rho_f = A_f / bd$ (1)	
$\rho_f = \alpha_1 \beta_1 \frac{f'_c}{f_{fu}} \frac{E_f \varepsilon'_c}{E_f \varepsilon'_c + f_{fu}}$ (2)	
$\alpha_1 = 0.85$ (3a)	$\alpha_1 = 0.85 - 0.0015 f'_c \geq 0.67$ (4a)
$\beta_1 = 0.85 - \frac{0.05(f'_c - 27.6)}{6.9}$ (3b)	$\beta_1 = 0.85 - 0.0025 f'_c \geq 0.67$ (4b)
$M_{u-theo} = \rho_f f_f b d^2 \left(1 - \frac{\rho_f f_f}{2\alpha_1 f'_c}\right)$ (5)	
$f_f = \sqrt{\frac{(E_f \varepsilon'_{cu})^2}{4} + \frac{0.85\beta_1 f'_c}{\rho_f} E_f \varepsilon'_{cu}} - 0.5 E_f \varepsilon'_{cu} < f_{fu}$ (6)	$f_f = A_f E_f \frac{\varepsilon'_{cu}(d-c)}{c} < f_{fu}$ (7)
	$\alpha_1 \beta_1 f'_c bc - A_f E_f \frac{\varepsilon'_{cu}(d-c)}{c} = 0$ (8)
$\Delta = \frac{(Pa/2)}{24 E_c I_e}\left[3L^2 - 4a^2\right]$ (9)	$\Delta = \frac{(P/2)L^3}{24 E_c I_{cr}}\left[3\frac{a}{L} - 4\left(\frac{a}{L}\right)^3 - 8\eta\left(\frac{L_g}{L}\right)^3\right]$ (12)
$I_e = \left(\frac{M_{cr}}{M_a}\right)^3 \beta_d I_g + \left[1 - \left(\frac{M_{cr}}{M_a}\right)^3\right] I_{cr} \leq I_g$ (10)	$\eta = 1 - \frac{I_{cr}}{I_g}$ (13)
$\beta_d = 0.2\left(\frac{\rho_f}{\rho_{fb}}\right) \leq 1.0$ (11)	

3.3 Comparison between GFRP-RGC andGFRP-RC beams

Table 8 shows the comparison between the normalized flexural capacity of GFRP-RGC and GFRP-RC beams. The GFRP-RC beams that were considered in the study have nearly similar dimensions, concrete strengths, and amount and type of reinforcements. In general, the bending-moment capacities of the tested beams (GFRP-RGC beams) were higher than the GFRP-RC beams owing to the enhanced mechanical properties of the geopolymer concrete compared with normal concrete, the provision of lateral ties within the constant bending-moment zone that provided confinement, and the higher tensile properties of GFRP bars used in this study compared with the previous ones.

Table 8. Flexural capacity of GFRP-RGC and GFRP-RC beams.

Reference	Beam	ρ_f (%)	$M_u / f'_c bd^2$
Current Study	GFRP-RGC-4-12.7	1.13	47.7
	GFRP-RGC-3-15.9	1.18	54.3
	GFRP-RGC-2-19.0	1.00	49.6
Toutanji and Saafi (14)	GB3-1	1.10	44.6
	GB3-2	1.10	47.3
Benmokrane et al. (15)	ISO1	1.10	35.1
	ISO2	1.10	36.7
Benmokrane et al. (16)	ISO30-2	1.01	35.9

4. Conclusions

The flexural response of geopolymer concrete beams reinforced with GFRP bars (GFRP-RGC beams) was investigated using a four-point static bending test. Based on the experimental results, the following conclusions were made:

- Nearly similar cracking pattern, load-deflection response, bending-moment and deflection capacities, and strain readings were obtained from all the tested beams. These results tend to show that the flexural performance of a GFRP-RGC beam is not dependent on the nominal diameter of the bottom longitudinal reinforcements.
- The uncracked and cracked response of the beams were relatively comparable since the strength of the beam mainly depends on the geopolymer concrete strength.
- The serviceability design criterion suggested by Bischoff et al. (0.3*MU-exp*) is more appropriate in designing a GFRP-RGC beam.
- The prediction equations recommended by ACI 440.1R-06 and CSA S806-12 underestimated the flexural and deflection capacities of the tested beams, suggesting that new prediction must be developed for a GFRP-RGC beam.
- The strength of GFRP-RGC beam is generally higher than that of GFRP-RC beam, indicating that the GFRP-RGC can be adapted for different structural applications; however, additional studies must be conducted to increase the approval of the proposed technology in the construction industry.

5. Acknowledgement

The authors would like to express their special thanks to V-ROD® Australia for providing the materials, the Natural Science and Engineering Research Council of Canada (NSERC), and the technical staff of the Centre of Excellence in Engineered Fibre Composites (CEEFC) at University of Southern Queensland.

6. References

1. Mehta, P. K., “Reducing the environmental impact of concrete”, Concrete International, 2001.
2. McCaffrey, R., “Climate change and the cement industry”. Global Cement and Lime Magazine (Environmental Special Issue, 2002, pp 15-19.

3. Davidovits, J., “Geopolymer chemistry and applications (3rd edition)” Institut Geopolymere, 2011, Saint-Quentin, France.
4. Rangan, B. V., Sumajouw, D. et al., “Reinforced low-calcium fly ash-based geopolymer concrete beams and columns”, Proceedings, 31st Conference on Our World in Concrete and Structures, 2006, Singapore.
5. Sofi, M., van Deventer, J. S. J. et al. “Bond performance of reinforcing bars in inorganic polymer concrete (IPC)”, Cement and Concrete Research, 37, 2007, pp. 251-257.
6. Duxson, P., Fernandez-Jimenez, A. et al. “Geopolymer technology: the current state of the art”, Journal of Material Science, 42, pp 2917-2933.
7. Gangarao, H. V. S., Taly N. et al., “Reinforced concrete design with FRP composites”, Taylor and Francis Group, 2007, NW, USA.
8. Canadian Standards Association, “Specification for fibre-reinforced polymers (CSA S807-10)”, CSA Group, 2010, Ontario, Canada.
9. American Concrete Institute, “Guide for the design and construction of building materials with fibre-reinforced polymers (ACI 440.1R-06)”, ACI Committee 440, 2006, Michigan, USA.
10. Canadian Standards Association, “Design and construction of building structures with fibre-reinforced polymers (CSA S806-12)”, CSA Group, 2010, Ontario, Canada.
11. Intelligent Sensing for Innovative Structures, “Reinforcing concrete structures with fibre reinforced polymers: Design Manual No. 3, Version 2”, ISIS Canada Corporation, 2006, Manitoba, Canada
12. Bischoff, P. H., Gross, S. et al., “The story behind the proposed changes to the ACI 440 deflection requirements for FRP-reinforced concrete”, ACI Special Publication, 264, 2009, pp 53-76.
13. El-Nemr A., Ahmed E. A. et al., “Evaluation of flexural behavior and serviceability performance of concrete beams reinforced with FRP bars”, ACI Structural Journal, 110, 2013, pp 1077-88.
14. Toutanji, H. A., Saafi, M., “Flexural behavior of concrete beams reinforced with glass fiber-reinforced polymer (GFRP) bars”, ACI Structural Journal, 97(5), 2000, pp 712-719.
15. Benmokrane, B., Chaallal, O. et al., “Flexural response of concrete beams reinforced with FRP reinforcing bars”, ACI Structural Journal, 1996, 91(2), pp 46-55.
16. Benmokrane, B., Chaallal, O. et al., “Glass fibre reinforced plastic (GFRP) rebars for concrete structures”, Construction and Building Materials, 1995, 9(6), pp 353-364.